

Use of Artificial Intelligence in Electrode Reaction Mechanism Studies: Application to the Thermodynamics and Kinetics of the Dissociation of Acetic Acid in Aqueous Solution

Haotian Chen^a, Danlei Li^a, Enno Kätelhön^b, Ruiyang Miao^a, Richard G. Compton^{a*}

^a Department of Chemistry, Physical and Theoretical Chemistry Laboratory, Oxford University, South Parks Road, Oxford OX1 3QZ, Great Britain

^b MHP Management- und IT-Beratung GmbH, Königsallee 49, 71638 Ludwigsburg, Germany

* Corresponding author.

Email address: Richard.compton@chem.ox.ac.uk (R. G. Compton)

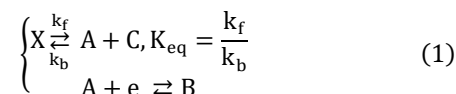
ABSTRACT: An artificial intelligence (AI) approach is developed for analysis of the voltammetry arising from a dissociative CE mechanism and applied to analyze experimental electrochemical data for the acetic acid dissociation in aqueous solution generating thermodynamic and kinetic data. Specifically, the variation of the steady state current for the reduction of protons at a platinum microelectrode as a function of the bulk concentration of acetic acid is recorded and analyzed giving data in quantitative agreement with independent measurements, provided the AI is trained with accurate and precise knowledge of diffusion coefficients of acetic acid, acetate ions and H^+ .

Introduction

Machine learning has, despite its enormous potential, been used only sporadically in the quantification of analytes in different electroanalytical contexts and less in fundamental electrochemistry. For example, in food chemistry, a support vector machine approach was used to distinguish ale from lager based on cyclic voltammetry, and a neural network was able to estimate alcoholic content¹. In environmental chemistry, along with cyclic square wave voltammetry, neural networks were applied to quantify the concentration of various pollutants in sea water, including copper, lead, mercury, paraquat (PQ) and Bisphenol-A (BPA)². In biosensor development, by integrating with fast-scan cyclic voltammetry (FSCV) and an autoencoder, a variant of an artificial neural network, Mao et al. impressively achieved in vivo quantification of the concentration of dopamine, ascorbate and NaCl in rat brains³. Multi-component detection of insulin and glucose in serum with the help of neural networks was also reported by Liu et al. recently⁴. Beyond chemical analysis, in fundamental electrochemistry, Bond et al. reported the successful classification of electrode reaction mechanisms (specifically E, EE and EC type processes) using a convolutional neural network⁵ and claimed recognition of electrode kinetic between Butler-Volmer and Marcus-Hush types using Bayesian inference⁶. More generally, at least in principle, when electrochemistry is equipped with machine learning for data analysis, the latter allows correlation and analysis of electrochemical data (including voltammograms and chronoamperograms) without the need for deploying mathematically analytical expressions.

Despite the emerging reports on the application to quantification of analytes, the study of electrochemical reactions and

mechanism with machine learning is still largely lacking. Bond and colleagues recently communicated the need for quantification of confidence limits and errors in parameter estimation when making a comparison of experimental data and simulated data. They attributed such absences to possible computational limitations⁷. In response to the desirability for machine learning of parameters in electrochemical reactions, we recently communicated the theoretical study of training neural networks on simulated voltammograms to infer rate/equilibrium constants from the voltammograms of a dissociative CE_{rev} reaction and the reverse process of predicting voltammograms from such constants without recourse to further simulation⁸. The general scheme of the dissociative CE reaction is:



where k_f and k_b are forward and reverse reaction rate constants respectively and the equilibrium constant, $K_{eq} = \frac{k_f}{k_b}$.

In this paper we next develop this work in the context of experiment and apply the approach to the extraction of thermodynamic and kinetic parameters for the acetic acid dissociation reaction in aqueous solution enabling comparison with extensive independent reports in the literature so permitting verification and critical evaluation of the AI approach including limitations.

Specifically, to facilitate proving the power of machine learning on parameter extraction from experiments, we quantitatively analyze current – concentration data to extract the thermodynamic and kinetic parameters (K_{eq} and k_f) of acetic acid dissociation using machine learning. The predicted parameters

are then checked via simulation and comparison of the results with experiments. Electro-reduction of acetic acid is known to follow a dissociative CE process^{9,10}:

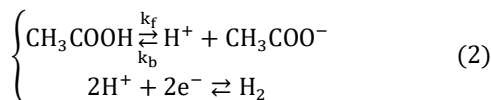


Table 1 shows the reported K_{eq} and k_f values at 298 K in different aqueous environments where the presence of added electrolyte is known to cause both kinetic and thermodynamic salt effects, albeit relatively small in magnitude (see Table 1). K_{eq} values of acetic acid are readily measured for example most simply from the pH of acetic acid solutions and reported as 1.754×10^{-5} M in pure water¹¹. Higher values are seen when electrolyte is present (i.e., 2.82×10^{-5} M in 0.1 M KCl solution¹²). Measurement of k_f has been made by a variety of methods.

Non-electrochemical methods reported include the electrical pulse methods¹³; the high field dispersion and temperature jump method¹⁴; and the electric field jump (E-jump) relaxation technique¹⁵. Although acetic acid does not absorb at visible wavelength, a colored acid-base indicator, Bromocresol green, was coupled in solution to enable spectroscopic detection using a square-wave field effect apparatus¹⁶.

Electrochemical methods reported include: voltammetry using a hydrodynamic modulated rotating disc electrode and analysis using the modified Koutecky-Levich equation^{9,17}; the polarography on acetate-acetic acid solution of low buffering capacity¹⁰; and a two-cell technique, each with a rotating electrode connected by Wheatstone bridge circuit¹⁸. A table of individually measured k_f and K_{eq} value is shown in Table 1. The values of k_f range widely from 1.91×10^5 to 3.46×10^6 s⁻¹ in different solution compositions.

Table 1. Literature Values of the Equilibrium and the Rate Constants of the Acetic Acid Dissociation Reaction.

constant	solution composition	value and reference
K_{eq} , M	CH ₃ COOH in pure water	1.754×10^{-5} , 11
	CH ₃ COOH, CH ₃ COONa in pure water	1.743×10^{-5} to 1.784×10^{-5} , 19
	CH ₃ COOH / 0.1106 M KCl(aq)	2.805×10^{-5} , 20
	CH ₃ COOH/ 0.1 M of KCl, NaCl or LiCl respectively	2.82×10^{-5} , 2.79×10^5 , 2.85×10^{-5} , 12
	CH ₃ COOH/1 M KCl(aq)	3.06×10^{-5} , 21
k_f , s ⁻¹ , non-electrochemical methods	0.1×10^{-3} M CH ₃ COOH in pure water	8×10^5 , 13
	8.3×10^{-5} M CH ₃ COOH in pure water	8.7×10^5 , 14
	CH ₃ COOH in pure water	1.91×10^5 , 15

	CH ₃ COOH coupled with Bromocresol blue in pure water	1.3×10^6 , 16
k_f , s ⁻¹ , electrochemical methods	2.7×10^{-3} M CH ₃ COOH, 0.03 M CH ₃ COONa / 1 M KCl	3.46×10^6 , 9
	2.17×10^{-3} M CH ₃ COOH / 1.475 M (CH ₃) ₄ N(Cl)	1.58×10^6 , 10
	20×10^{-3} M CH ₃ COOH / 0.1 and 0.3 M KCl	9.1×10^5 , 18
	CH ₃ COOH / 1 M KCl(aq)	3×10^5 , 22
	2.5×10^{-3} M CH ₃ COOH, 5×10^{-3} M CH ₃ COONa / 50:50 water-ethanol. Ionic strength adjusted to 1 M with KCl	2.9×10^5 , 23
	CH ₃ COOH/LiCl(aq) . Ionic strength adjusted to 1 M with LiCl	1.39×10^6 , 24, 25

In the following we report a simple three-step electrochemical approach for estimating these two constants.

First, measurements are made of the steady state current for the reduction of protons as a function of the bulk acetic acid concentration, $C_{\text{CH}_3\text{COOH},\text{total}}$ at a Platinum microdisc electrode. This approach was preferred to cyclic voltammetry because the steady state currents obtained at a microelectrode are independent of electrochemical rate constants and transfer coefficients whereas understanding and simulating a full voltammogram either at a macroelectrode or a micro-electrode for the reduction of H⁺ from acetic acid dissociation would require a confident knowledge of the mechanism and the kinetic parameters of the hydrogen evolution reaction on Pt electrode, which remains controversial^{26,27}. Under the conditions employed in the present study, the steady state current depends only on k_f , K_{eq} , and $C_{\text{CH}_3\text{COOH},\text{total}}$ assuming prior knowledge of diffusion coefficients.

Second, simulation of the expected limiting currents with different k_f , K_{eq} and bulk concentration of acetic acids was conducted to obtain the steady state current under different conditions and a neural network was trained and tested with simulated data. The features used for training were the steady state currents at different bulk concentrations of acetic acid and targets were the k_f and K_{eq} values for the acetic acid CE process.

Third, steady state currents obtained from experiments were fed into the trained network to give predictions of k_f and K_{eq} values which were compared with those in Table 1 facilitating generic insights into the AI approach.

Theory

In this section we first discuss the formal potential of the H⁺/H₂ couple and the expected half-wave potential for the reduction of protons in the case that if the proton reduction reac-

tion is electrochemically reversible. Second we outline the simulation of the expected transport limited currents for the proton reduction as a function of K_{eq} and k_f , noting that computational approach is given in reference ⁸ apart from small changes in boundary conditions as outlined below.

Formal Potential and half wave potential of the H^+/H_2 couple. The formal potential, $E_{f,H^+/H_2}^0$ of the H^+/H_2 couple has been shown to be given by:

$$E_{f,H^+/H_2}^0 = E_{H^+/H_2}^0 + \frac{RT}{F} \ln \frac{\gamma_{H^+} \sqrt{p^0}}{\sqrt{K_{H_2} 10^{k_s c_s} a^0}} \quad (3)$$

where E_{H^+/H_2}^0 is the standard electrochemical potential, γ_{H^+} is the activity coefficient of H^+ ion in solution. k_s and c_s are the salt parameter and salt concentration respectively which accounts for salt-out effect in an electrolytic solution. p_0 and a_0 are standard pressure and standard activity which are 1 bar and 1 M respectively. K_{H_2} is the Henry's law constant for H_2 . R , T and F are gas constant, temperature and Faraday constant respectively. Using parameters from Table 2, $E_{f,H^+/H_2}^0$ is calculated as -0.341 V vs. SCE ²⁸.

The half wave potential assuming an electrochemically reversible H^+/H_2 couple for the reduction of protons at a uniformly accessible electrode has been derived previously²⁸:

$$E_{1/2} = \frac{\frac{1}{2} \ln \left(\frac{c_{H^+}^* D_{H_2}}{c^0 D_{H^+}} \right) RT}{F} + E_{f,H_2/H^+}^0 \quad (4)$$

where $E_{1/2}$ is half wave potential and $c_{H^+}^*$ and c^0 are the bulk concentration of acetic acid and reference concentration (1 M) respectively. The dependence of the half-wave potential on the bulk proton concentration arises from the non-unity stoichiometry of the reaction^{28, 29}. The formal potential, $E_{f,H^+/H_2}^0$ as derived above is -0.341 V vs. SCE. Using the reported pK_a value of 4.756 of acetic acid¹¹ and bulk concentration of acetic acid as 10 mM, $c_{H^+}^*$ is calculated to be 4.10×10^{-4} M and $E_{1/2}$ is estimated as -0.448 V vs. SCE. On the other hand, assuming $c_{H^+}^*$ as the bulk concentration of acetic acid, the calculated $E_{1/2}$ is -0.408 V vs. SCE. Clearly from the CE process with describing the acetic acid reduction with the hypothetical assumption of reversible electrochemistry, the half wave potential would be expected to lie between -0.408 to -0.448 V.

Table 2. Parameters Used for Calculation of the Formal Potential of the H^+/H_2 Redox Couple and for Simulation.

parameter	explanation	value
E_{H^+/H_2}^0 vs. SCE	standard potential of H^+/H_2 vs. saturated calomel electrode	-0.241 V, ³⁰
D_{CH_3COOH}	diffusion coefficient of acetic acid	$1.29 \times 10^{-9} \text{ m}^2 \text{ s}^{-1}$, ¹¹
$D_{CH_3COO^-}$	diffusion coefficient of acetate	$1.089 \times 10^{-9} \text{ m}^2 \text{ s}^{-1}$, ¹¹
D_{H^+}	diffusion coefficient of Hydrogen ion	$9.311 \times 10^{-9} \text{ m}^2 \text{ s}^{-1}$, ¹¹
D_{H_2}	diffusion coefficient of Hydrogen	$5.11 \times 10^{-9} \text{ m}^2 \text{ s}^{-1}$, ¹¹

γ_{H^+}	Activity coefficient of Hydrogen ion	0.754, ³¹
K_{H_2}	Henry's Law constant of hydrogen	1292 bar M^{-1} , ³²
c_{KNO_3}	concentration of KNO_3 electrolyte in experiment	0.1 M
k_{KNO_3}	salt parameter of KNO_3	0.07 M^{-1} , ³³

Simulation equations. The mass transport is assumed to be exclusively diffusive, and the diffusion equations coupled with chemical reactions are solved to show how the steady-state limiting current at a microelectrode depends on the parameters k_f and K_{eq} for different acetic acid concentrations. Note that the electrochemical reaction on a microdisc electrode of radius r can be approximated as a hemispherical electrode with radius $\frac{2r}{\pi}$ to reduce the diffusion problem from two dimensions to one dimension. The relevant steady state diffusion equations can be formulated as:

$$\begin{cases} 0 = D_{CH_3COOH} \frac{\partial^2 [CH_3COOH]}{\partial r^2} + \frac{2}{r} \frac{\partial [CH_3COOH]}{\partial r} - k_f [CH_3COOH] + k_b [H^+] [CH_3COO^-] \\ 0 = D_{H^+} \frac{\partial^2 [H^+]}{\partial r^2} + \frac{2}{r} \frac{\partial [H^+]}{\partial r} + k_f [H^+] - k_b [H^+] [CH_3COO^-] \\ 0 = D_{H_2} \frac{\partial^2 [H_2]}{\partial r^2} + \frac{2}{r} \frac{\partial [H_2]}{\partial r} \\ 0 = D_{CH_3COO^-} \frac{\partial^2 [CH_3COO^-]}{\partial r^2} + \frac{2}{r} \frac{\partial [CH_3COO^-]}{\partial r} + k_f [H^+] - k_b [H^+] [CH_3COO^-] \end{cases} \quad (5)$$

where D_j is the diffusion coefficient for species j .

If r_e is the radius of the hemispherical electrode, the boundary conditions at the surface of electrode for the steady state reduction of protons:

$$r = r_e \begin{cases} D_{CH_3COOH} \left(\frac{\partial [CH_3COOH]}{\partial r} \right)_{r=r_e} = 0 \\ [H^+]_{r=r_e} = 0 \\ D_{CH_3COO^-} \left(\frac{\partial [CH_3COO^-]}{\partial r} \right)_{r=r_e} = 0 \end{cases} \quad (6)$$

The boundary conditions for the outer boundary of simulation are:

$$r = r_{sim} \begin{cases} c_{CH_3COOH}^* = c_T - \frac{-K_{eq} + \sqrt{K_{eq}^2 + 4c_T K_{eq}}}{2} \\ c_{H^+}^* = \frac{-K_{eq} + \sqrt{K_{eq}^2 + 4c_T K_{eq}}}{2} \\ c_{H_2}^* = 0 \\ c_{CH_3COO^-}^* = \frac{-K_{eq} + \sqrt{K_{eq}^2 + 4c_T K_{eq}}}{2} \end{cases} \quad (7)$$

where $c_T = c_{CH_3COOH, total}$ is the concentration of acetic acid added to the solution before chemical equilibrium forming proton and acetate, which are assumed absent in the initial solution. In the absence of electrolysis, $c_{CH_3COOH, total} = c_{CH_3COOH}^* +$

$c_{\text{CH}_3\text{COO}^-}^*$ and r_{sim} is the outer boundary of the simulation as discussed in reference⁸.

EXPERIMENTAL

Chemicals. Acetic acid (CH_3COOH , 99.8%), potassium nitrate (KNO_3 , 99%), potassium chloride (KCl , 99%) and hexaammineruthenium (III) chloride ($\text{Ru}(\text{NH}_3)_6\text{Cl}_3$, 98%) were purchased from Sigma-Aldrich (Dorset, UK) and used as received. All solutions were prepared with deionized water (of resistivity 18.2 $\text{M}\Omega\text{ cm}$ at 298 K, Millipore).

Voltammetry and chronoamperometry of acetic acid at a Pt microdisc electrode. All electrochemical measurements were performed with a $\mu\text{Autolab}$ Type III potentiostat analyzer using a standard three electrode arrangement in an optimized and thermostatted electrochemical cell³⁴ in a Faraday cage. A Pt microdisc electrode (diameter: approximately 10 μm) was polished with three grades of successively finer aluminum powder (1.0, 0.3 and 0.05 μm), washed with deionized water, dried with N_2 flow and served as the working electrode. The counter and reference electrodes were a platinum wire and a saturated calomel electrode (SCE) respectively. The radius of Pt microdisc electrode was calibrated electrochemically as $4.97 \pm 0.05 \mu\text{m}$ by analyzing the steady state voltammetry of 1.0 mM $[\text{Ru}(\text{NH}_3)_6]^{3+}$ in 0.1 M KCl aqueous solution, using the reported diffusion coefficient for $[\text{Ru}(\text{NH}_3)_6]^{3+}$ of $8.43 \times 10^{-10} \text{ m}^2/\text{s}$ at 298 K in 0.1 M KCl solution³⁵.

Acetic acid solutions with four concentrations (10, 20, 40 and 100 mM) were prepared in 0.1 M KNO_3 supporting electrolyte. The solution was degassed for 10 minutes with N_2 before voltammetric or chronoamperometric measurements and temperature stabilized at $298 \pm 1 \text{ K}$ via a digital temperature controller (SCT1 Digital contact thermometer)³⁴. Current time transients for analysis via AI were recorded at an applied potential of -1.0 V vs. SCE for a duration of 10 seconds. The working electrode was polished with 0.05 μm aluminum powder and washed with deionized water between each experiment. Three repeat chronoamperometries were performed for each concentration.

SIMULATION AND MACHINE LEARNING

The simulation program was written in Python. Multiprocessing was used for parallel computing of the working surfaces on an Intel E5 processor. The non-linear diffusion equations were solved using the finite difference method by discretizing the diffusion equations using both expanding space grid and time grid. The resulting multi-diagonal matrix was solved using the Newton-Raphson method for at most 10 iterations³⁶. If the mean absolute error in dimensionless concentration was smaller than 10^{-12} , additional iterations were skipped to save time without significant compromise of accuracy. The convergence of the simulation was checked, and the results can be found in Testing and Verification of the Simulations section in the Supporting Information³⁷⁻³⁹.

The working surfaces from simulations were used to train a multiheaded Dense Neural Network (DNN) written in TensorFlow⁴⁰. The DNN was trained by using the simulated steady state currents at different concentrations as features to predict the corresponding $\log_{10} k_f$ and $\log_{10} K_{\text{eq}}$ as targets. Note that the targets were in logarithm form to reduce the exploding/di-

minishing gradient problem⁴¹. The DNN has only 4 hidden layers with relatively small numbers of neurons (<100) to avoid overfitting: a smaller network forced itself to predict rate constants instead of ‘memorizing’ them.

RESULTS AND DISCUSSION

First, linear sweep voltammetry of 10 mM acetic acid in 0.1 M KNO_3 was performed in the potential range from -0.15 to -1.0 V vs. SCE. Figure 1 shows a voltammogram measured at 800 mV/s from which a halfwave potential of -0.570 V vs. SCE, was inferred and is similar to the value reported elsewhere for analogous experiments using a Pt microelectrode⁴². The value can be compared with the estimated half wave potential assuming an electrochemically reversible H^+/H_2 couple which was derived above and expected to lie between -0.408 to -0.448 V. However, as shown in Figure 1, the half peak wave found in experiment showed significant overpotential suggesting that the reduction of H^+ on Pt microdisc electrode was at least partly electrochemically irreversible²⁸, consistent with previous observations⁴³⁻⁴⁶.

The voltammogram shown in Figure 1 contains information about the solution phase chemistry, notably the thermodynamics and kinetics of the acetic acid dissociation, as well as the electrode kinetics of the proton reduction reaction. The latter in turn reflects the complexity of the multistep reaction which is known to involve adsorbed hydrogen probably located on different sites on the Platinum electrode surface^{26, 27}. Despite extensive study, the mechanistic and kinetic details remain open to debate^{27, 47-50}. Since the aim of the present study is the extraction of the values of k_f and K_{eq} describing the acetic acid dissociation instead of analyzing the entire voltammetric wave using AI, we focused on the steady state limiting current only, which is necessarily independent of the details of the electrode kinetics such as the standard electrochemical rate constant, k_0 , and the transfer coefficient, α . Under these conditions the steady state current only depends on k_f , K_{eq} , and $c_{\text{CH}_3\text{COOH},\text{total}}$ assuming prior knowledge of the diffusion coefficients of the different species. For this purpose, measurements were made at potential of -1.0 V vs. SCE corresponding to the limiting current and the attainment of the steady state current assessed by chronoamperometry as described in the next section. Specifically, the measurement of the limiting current as a function of the bulk concentration of acetic acid is used to avoid the need for any electrode kinetic data or assumption.

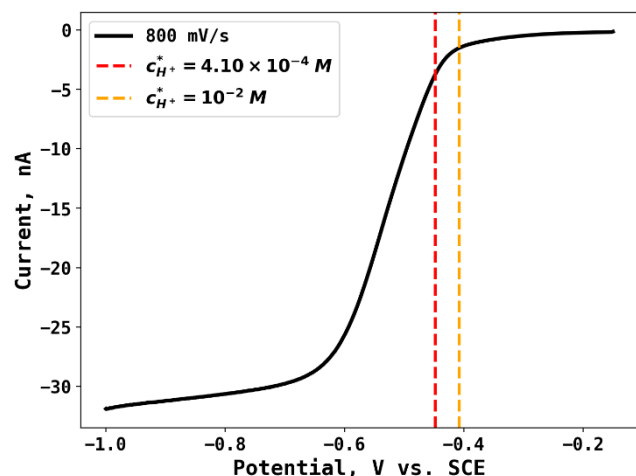


Figure 1. The linear sweep voltammetry of 10 mM acetic acid in 0.1 M KNO_3 at a scan rate of 800 mV/s from -0.15 to -1.0 V vs. SCE. Dashed lines show the calculated half wave potentials at different bulk concentrations of H^+ (see text).

Chronoamperometry of acetic acid. To identify the steady state currents, current-time transients for four different concentrations of acetic acid between 10 and 100 mM in 0.1 M KNO_3 were recorded at a Pt microdisc electrode by stepping the potential from a value where no current flowed to an applied potential of -1.0 V vs. SCE, corresponding to a sufficiently negative potential for a diffusion limited reduction of protons. Figure 2 shows the corresponding chronoamperograms recorded for a period of 10 seconds (purple – 10 mM, blue – 20 mM, green – 40 mM and yellow – 100 mM). From Figure 2, they were deemed to have effectively reached steady state behavior after 2 seconds.

Erring on the side of caution, currents at $t = 10$ s were chosen for quantitative analysis, assumed to be steady state and measured as -30.5 ± 0.4 , -55.2 ± 0.3 , -102 ± 1 and -238 ± 4 nA for 10.0, 20.0, 40.0 and 100 mM of acetic acid with three separate chronoamperograms averaged for each concentration. The steady state currents did not scale proportionally with concentration of acetic acid since the reduction of acetic acid obeys the dissociative CE mechanism. The concentrations of acetic acid and the measured steady state currents were utilized as experimental features for machine learning to predict rate and equilibrium constant as described below.

Simulation of steady-state limiting currents. A wide range of k_f (1 to 10^8 s $^{-1}$) and K_{eq} (10^{-3} to 10^{-8} M) values were applied to simulate the steady state limiting currents at four different bulk concentrations of acetic acid (10, 20, 40, and 100 mM). The diffusion coefficients of all species reported in the literature and given in Table 2. Note that some combinations of K_{eq} and k_f values would generate k_b values exceeding a reasonable magnitude, so simulations were only performed if $k_b \leq 10^{13}$ M $^{-1}$ s $^{-1}$ with the latter values selected to give a considerable margin of error. The steady state currents at different k_f and K_{eq} values are represented on the working surfaces such as the one shown in Figure 3 for a bulk concentration of acetic acid of 10 mM. Figure 3 shows that the steady state current increases in magnitude with increasing K_{eq} and k_f . Increasing K_{eq} can increase the magnitude of steady state current since higher K_{eq} increases the bulk concentration of electroactive H^+ at equilibrium. Higher k_f increases the extent of acetic acid dissociation on the voltammetric timescale to replenish H^+ consumed during electrochemical reduction. The working surfaces for bulk concentrations of acetic acid of 20, 40 and 100 mM can be found in the Working Surfaces for the Steady-State Limiting Current in the Supporting Information.

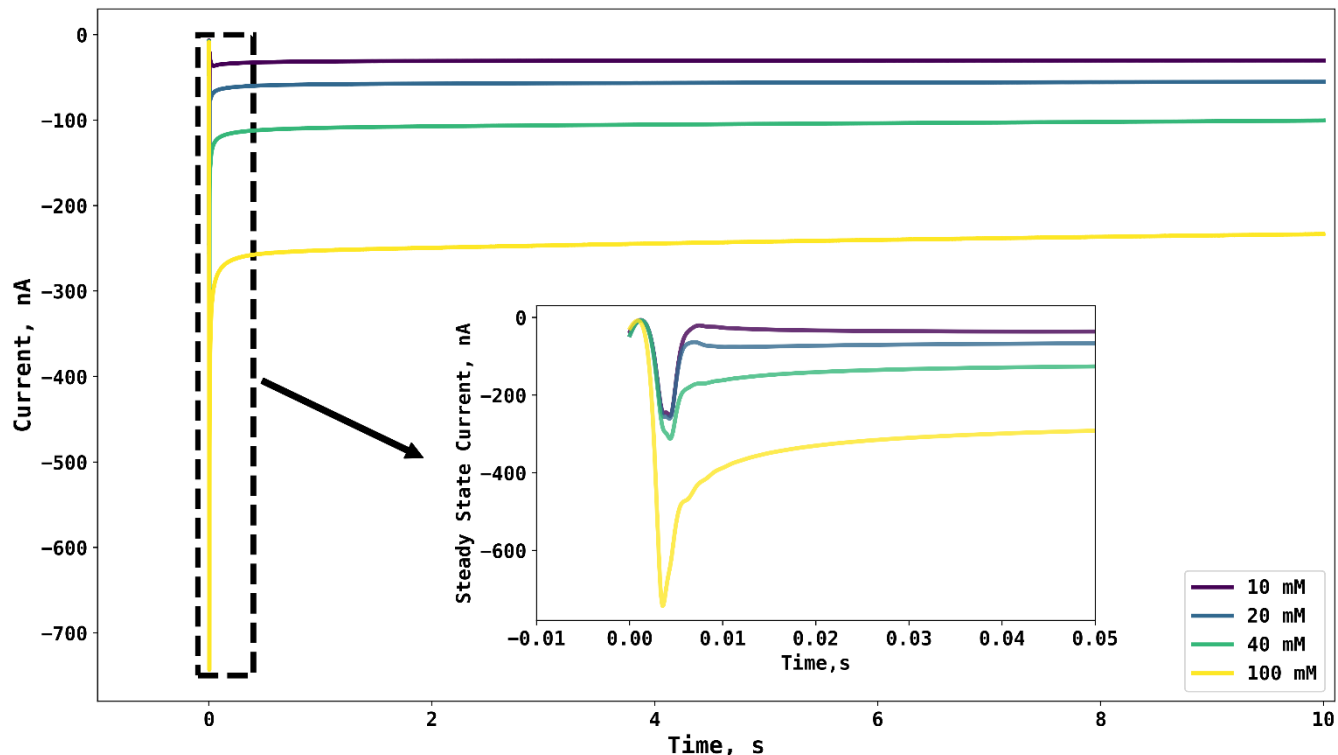


Figure 2. Chronoamperometry of different concentrations of acetic acid in 0.1M KNO_3 at a Pt microdisc electrode at 298 K. The duration of chronoamperometry scan was 10 seconds and the applied potential was -1.0 V. The inset figure is a zoom-in view of the chronoamperogram from 0 to 0.05 seconds.

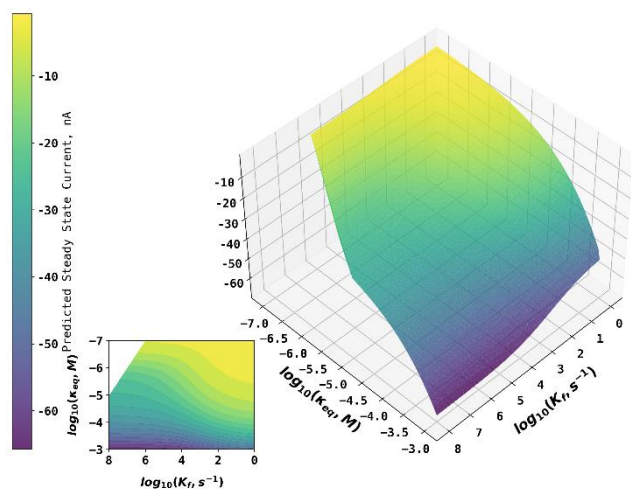


Figure 3. The working surface showing the steady state currents at different k_f and K_{eq} values for a bulk concentration of acetic acid of 10 mM. Note: the apparent 'kink' in the left of the surface is because it is not parallel to the $\log_{10} K_{eq}$ axis but rather cross (k_f and K_{eq}) space at an angle. The smooth continuity of the surface is emphasized by the contour plot.

Training and testing the neural network. Using the working surfaces, the neural network was trained to predict $\log_{10} k_f$ and $\log_{10} K_{eq}$ using steady state currents at four different concentrations of acetic acid and trained for 2000 epochs.

The loss function was the mean absolute error (MAE) and the optimizer was Adam (learning rate = 0.001)⁵¹. To evaluate the performance of the neural network model after training, it was tested with independent testing datasets and the results are shown in Figure 4, as 90.5% of predictions of $\log_{10} k_f$ were within 10% error and 100% of predictions of $\log_{10} k_f$ were within 10% error. The lower accuracy of predictions of $\log_{10} k_f$ compared to $\log_{10} K_{eq}$ arises because $\log_{10} k_f$ had relatively smaller effect on the steady state current but the network was judged sufficient for prediction of constants from experimental results.

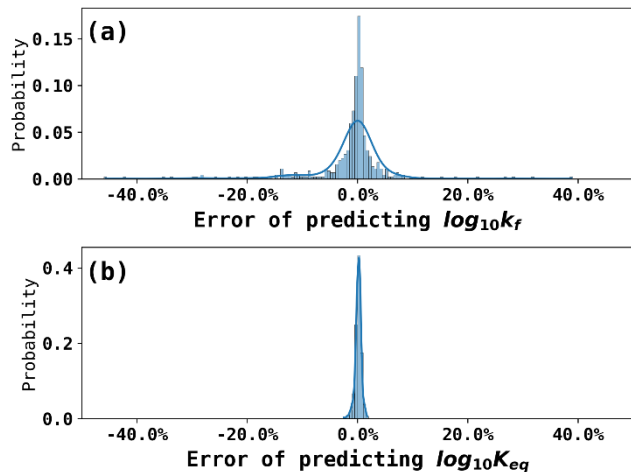


Figure 4. Error of predicting rate and equilibrium constants from an independent testing dataset composed of simulated steady state currents. (a) errors of predicting $\log_{10} k_f$. 90.5% of predictions of $\log_{10} k_f$ were within 10% errors; (b) errors of predicting $\log_{10} K_{eq}$. 100% of predictions of $\log_{10} K_{eq}$ were within 10% errors.

Predicting rate and equilibrium constants with experimental data. Using the steady state current at the four different concentrations as input of the neural network trained in the last step, the neural network predicted k_f and K_{eq} values in logarithmic scale as 6.47 and -4.77 which convert to $2.95 \times 10^6 \text{ s}^{-1}$ and $1.70 \times 10^{-5} \text{ M}$. The 95% prediction intervals for the of neural network were estimated using the bootstrap method⁵². First, 500 observations were sampled from testing datasets and repeated for 100 times to obtain 100 bootstrapped samples. Second, each bootstrap sample was trained in an independent neural network to obtain an empirical distribution of bootstrap predictions. At 5% significance level, the upper and lower limit were 97.5 and 2.5% quantile obtained from the bootstrap distribution. The 95% prediction interval were calculated as 2.78×10^6 to $3.13 \times 10^6 \text{ s}^{-1}$ and 1.67×10^{-5} to $1.71 \times 10^{-5} \text{ M}$ for predicted k_f and K_{eq} respectively. These values are fully consistent with the accepted literature values shown in Table 1 showing the power of the proposed AI approach in extracting kinetic and thermodynamic data.

Testing the approach with different diffusion coefficients. Not all systems under study will have as well characterized diffusion coefficient as the acetic acid dissociation reaction described above. Sometimes, diffusion coefficients are unknown and frequently uncertain. It is therefore pertinent to ask how well the AI approach responds to variations in the diffusion coefficients used for the proton, acetic acid and acetate ions.

To address this question we compared the performance of the three-step electrochemical approach with five different set of diffusion coefficients as shown in Table 3: (case 1) diffusion coefficients as reported in Table 2; diffusion coefficients as reported in Table 2 but increased by 10% (case 2) or decreased by 10% (case 3); (case 4) diffusion coefficients of all species arbitrarily set as $10^{-9} \text{ m}^2 \text{ s}^{-1}$; (case 5) D_{H^+} assigned the literature value of $9.311 \times 10^{-9} \text{ m}^2 \text{ s}^{-1}$ (see Table 2) and the diffusion coefficients of other species as $10^{-9} \text{ m}^2 \text{ s}^{-1}$. The simulated

steady state currents in each case were used for machine learning and the predicted k_f and K_{eq} were: (case 1) $k_f = 2.95 \times 10^6 \text{ s}^{-1}$, $K_{eq} = 1.70 \times 10^{-5} \text{ M}$; (case 2) $k_f = 3.02 \times 10^3 \text{ s}^{-1}$, $K_{eq} = 5.13 \times 10^{-6} \text{ M}$; (case 3) $k_f > 10^{10} \text{ s}^{-1}$, $K_{eq} = 3.47 \times 10^{-6} \text{ M}$; (case 4) $k_f = 9.05 \times 10^2 \text{ s}^{-1}$, $K_{eq} = 1.56 \times 10^{-3} \text{ M}$; (case 5) $k_f > 10^{10} \text{ s}^{-1}$, $K_{eq} = 1.07 \times 10^{-5} \text{ M}$. The values for k_f and K_{eq} obtained for the wrong diffusion coefficients which deviate from the accepted values give noticeably wrong answers.

Table 3. The 5 Cases Considered When Varying Diffusion Coefficients of Species and the Predicted k_f and K_{eq} Values.

case #	description	predicted k_f, s^{-1}	predicted K_{eq}, M
1	diffusion coefficients shown in Table 2	2.95×10^6	1.70×10^{-5}
2	increasing diffusion coefficients in Table 2 by 10%	3.02×10^3	5.13×10^{-6}
3	decreasing diffusion coefficients in Table 2 by 10%	$> 10^{10}$	3.47×10^{-6}
4	all diffusion coefficients set to $10^{-9} \text{ m}^2 \text{ s}^{-1}$	9.05×10^2	1.56×10^{-3}
5	$D_{H^+} = 9.311 \times 10^{-9} \text{ m}^2 \text{ s}^{-1}$, other species $10^{-9} \text{ m}^2 \text{ s}^{-1}$	$> 10^{10}$	1.07×10^{-5}

In cases 2 and 3 the diffusion coefficients were arbitrarily set higher or lower than the accepted values by 10%. The effect is that for lowered diffusion coefficients the K_{eq} and k_f values increase to provide more or more rapid dissociation whilst for increased diffusion coefficients, the opposite occurs and the two parameters decrease to reduce the number of protons formed through dissociation on the voltammetric timescale. These trends are exactly what is expected since we are using the limiting current to probe the two parameters of interest and so the inferred values will be very sensitive to the rate of diffusion in addition to k_f and K_{eq} . The steady state concentration profiles of CH_3COO^- , H^+ and CH_3COOH in in case 1, 2 and 3 are shown in Figure 5 when (a) $c_{\text{CH}_3\text{COOH}, \text{total}}^* = 100 \text{ mM}$ and (b) $c_{\text{CH}_3\text{COOH}, \text{total}}^* = 10 \text{ mM}$.

It is interesting first that the values of k_f and K_{eq} are changed so markedly, highlighting a limitation of the electrochemical method for their measurement and second that the AI approach stresses the requirement for accurate parameter input in a way which is much more emphatic than using traditional curve fitting approaches.

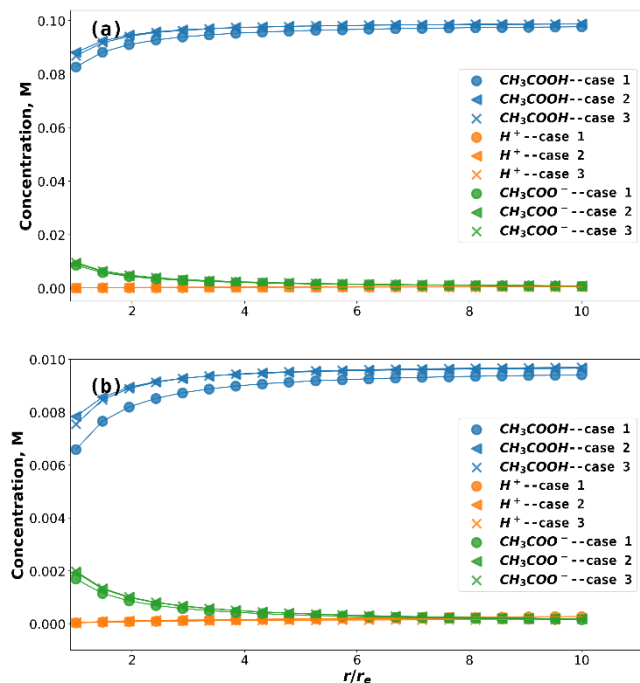


Figure 5. Simulated steady state concentration profile for case 1, 2, and 3. (a) $c_{CH_3COOH,total}^* = 100 \text{ mM}$; (b) $c_{CH_3COOH,total}^* = 10 \text{ mM}$ (see text and Table 3).

In the example chosen for study, all three diffusion coefficients are well known and the used in case 1 are considered to be reliably especially as they are measured via conductivity or Gouy interferometry⁵³. In some cases where the diffusion coefficients are unknown, an experimenter might be tempted to estimate or guess the relevant parameters. Thus, in case 4 and 5 we investigate this approach and fix some or all for the diffusion coefficients as $10^{-9} \text{ m}^2 \text{ s}^{-1}$. The use of this pathologically low set of values leads to unrealistically high values of k_f in particular. The steady state concentration profiles of CH_3COO^- , H^+ and CH_3COOH in case 1, 4 and 5 are shown in Figure 6 when (a) $c_{CH_3COOH,total}^* = 100 \text{ mM}$ and (b) $c_{CH_3COOH,total}^* = 10 \text{ mM}$ and are to be contrasted with those generated from more reliable diffusion coefficients.

The five cases discussed above showed that incorrect simulation parameters, notably diffusion coefficients lead to incorrect input data for the neural network training and generate unreliable predictions. Thus, in practice, we recommend major caution with simulation parameters for accurate simulations and predictions.

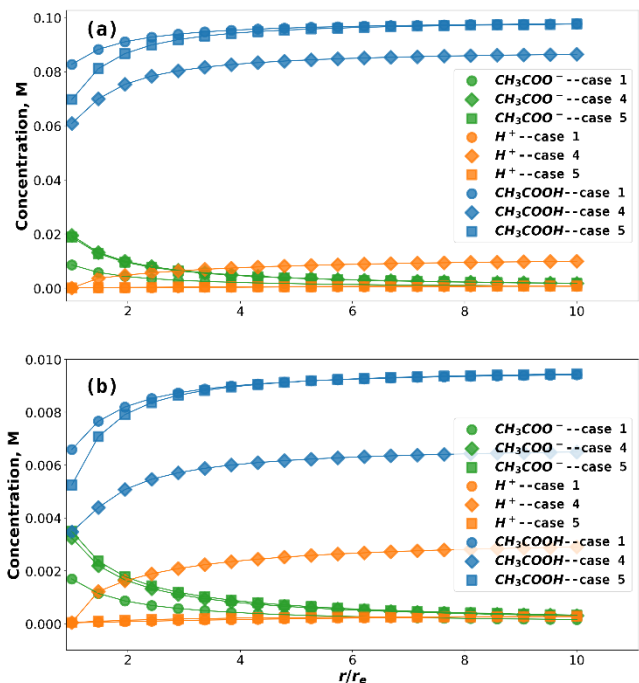


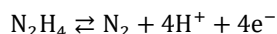
Figure 6. Simulated steady state concentration profile for case 1, 4, and 5. (a) $c_{CH_3COOH,total}^* = 100 \text{ mM}$; (b) $c_{CH_3COOH,total}^* = 10 \text{ mM}$ (see text and Table 3).

CONCLUSIONS

We have shown how Artificial Intelligence methods can be developed and trained to analyze electrochemical data and extract reliable kinetic and thermodynamic parameters which compare well with those independently measured both by electrochemical and non-electrochemical methods. The specific approach previously advocated⁸ has been shown to be effective when using simulation to train and validate AI programs and then applied to authentic experimental data. However, it is useful to assess the strengths and especially the limitations of the approach. We note that the method meets the challenge presented by Bond and colleagues in giving a well-defined and experimenter – independent method of data analysis. However, it must be recognized that we have applied it to a well-defined system where the mechanism of electrode process under evaluation is known. This is required to perform the simulation necessary to train the AI. Moreover, because the chemistry is clear it is possible to simplify the number of parameters needed for training by adopting the reliable literature data for the diffusion coefficients of the 3 species controlling the magnitude of the current, acetic acid, acetate ions and protons. Even so from the analysis using deliberately wrong diffusion coefficients it is clear that even relatively small errors in the values leads to significant error in the inferred k_f and K_{eq} values. That said AI allows the sensitivity of the values to be readily checked and the inferences caveated in a way which is not always easily adopted in conventional analysis of voltammogram.

It is evident that the approach of using simulation to train the AI requires a clear understanding of the likely chemistry even

if the experimenter is willing to simulate and train AI for different possible mechanisms. Overall this points to a possible need to make complementary measurements, notably spectro-electrochemistry, and/or good chemical intuition to identify realistic chemistry. In the above we deliberately selected to focus our analysis on the limiting current data from our experiments to make our conclusion independent of the mechanism and electrode kinetics of the H^+/H_2 redox couple which would influence cyclic voltammetric data (peak current, peak potentials). The speculative application of a trained network for more complex chemistry is fraught with risk, possibly extreme risk. Thus, in the context of dissociative CE mechanism such as a process undoubtedly underpins the oxidation of hydrazine in aqueous solution where deprotonation of N_2H_5^+ prior to oxidation of N_2H_4 is required at some electrodes however the oxidation process is self-inhibiting since it produces nitrogen and protons^{54, 55}.



which act to change the pH of the solution local to the electrode. The application of an AI program trained for a simple dissociative CE process could not capture the essential content of the voltammetry/chronoamperometry and requires chemical expertise from the experimenter. Similarly, the voltammetry of blood reveals signals attributed to the electro-reduction of oxygen released from oxy-hemoglobin close to an electrode⁵⁶⁻⁵⁸. Again, the chemistry is not simple: four oxygen molecules are bound to each hemoglobin and have different kinetics and thermodynamics of release. A chemically over-simplified analysis using AI trained for a simple mechanism would likely gave erroneous or misleading output. We predict that the role of Human Intelligence ('HI') will remain dominant over the Artificial form for the foreseeable future in electrochemistry at least except for some niche applications!

ASSOCIATED CONTENT

Supporting Information

The Supporting Information is available free of charge at XXX.

Testing and verification of the simulations; Working surfaces of steady state limiting current

AUTHOR INFORMATION

Corresponding Author

Richard G. Compton – Department of Chemistry, Physical and Theoretical Chemistry Laboratory, Oxford University, South Parks Road, Oxford OX1 3QZ, Great Britain; Email: Richard.compton@chem.ox.ac.uk

Authors

Haotian Chen – Department of Chemistry, Physical and Theoretical Chemistry Laboratory, Oxford University, South Parks Road, Oxford OX1 3QZ, Great Britain

Danlei Li – Department of Chemistry, Physical and Theoretical Chemistry Laboratory, Oxford University, South Parks Road, Oxford OX1 3QZ, Great Britain

Enno Kätelhön – MHP Management- und IT-Beratung GmbH, Königsallee 49, 71638 Ludwigsburg, Germany

Ruiyang Miao - Department of Chemistry, Physical and Theoretical Chemistry Laboratory, Oxford University, South Parks Road, Oxford OX1 3QZ, Great Britain

Author Contributions

All authors have given approval to the final version of the manuscript.

ACKNOWLEDGMENT

Haotian Chen thanks Lady Margaret Hall for a 2020/2021 Postgraduate Scholarship Award.

REFERENCES

1. Roselló, A.; Serrano, N.; Díaz-Cruz, J. M.; Ariño, C., Discrimination of Beers by Cyclic Voltammetry Using a Single Carbon Screen-printed Electrode. *Electroanalysis* **2021**, *33* (4), 864-872.
2. Dean, S. N.; Shriver-Lake, L. C.; Stenger, D. A.; Erickson, J. S.; Golden, J. P.; Trammell, S. A., Machine Learning Techniques for Chemical Identification Using Cyclic Square Wave Voltammetry. *Sensors* **2019**, *19* (10), 2392.
3. Mao, L.; Xue, Y.; Ji, W.; Jiang, Y.; Yu, P., Deep learning for voltammetric sensing in living animal brain. *Angew. Chem.* **2021**.
4. Zhao, Y.; Zhang, H.; Li, Y.; Yu, X.; Cai, Y.; Sha, X.; Wang, S.; Zhan, Z.; Xu, J.; Liu, L., AI powered electrochemical multi-component detection of insulin and glucose in serum. *Biosens. Bioelectron.* **2021**, *186*, 113291.
5. Kennedy, G. F.; Zhang, J.; Bond, A. M., Automatically Identifying Electrode Reaction Mechanisms Using Deep Neural Networks. *Anal. Chem.* **2019**, *91* (19), 12220-12227.
6. Li, J.; Kennedy, G. F.; Gundry, L.; Bond, A. M.; Zhang, J., Application of Bayesian Inference in Fourier-Transformed Alternating Current Voltammetry for Electrode Kinetic Mechanism Distinction. *Anal. Chem.* **2019**, *91* (8), 5303-5309.
7. Bond, A. M., A perceived paucity of quantitative studies in the modern era of voltammetry: prospects for parameterisation of complex reactions in Bayesian and machine learning frameworks. *J. Solid State Electrochem.* **2020**, *24* (9), 2041-2050.
8. Chen, H.; Kätelhön, E.; Le, H.; Compton, R. G., Use of Artificial Intelligence in Electrode Reaction Mechanism Studies: Predicting Voltammograms and Analyzing the Dissociative CE Reaction at a Hemispherical Electrode. *Anal. Chem.* **2021**.
9. Kanzaki, Y.; Tokuda, K.; Bruckenstein, S., Dissociation rates of weak acids using sinusoidal hydrodynamic modulated rotating disk electrode employing Koutecky-Levich equation. *J. Electrochem. Soc.* **2014**, *161* (12), H770.
10. Schroeder, R. R.; Shain, I., Application of the potentiostatic method. Determination of the rate constant for the dissociation of acetic acid. *J. Phys. Chem.* **1969**, *73* (1), 197-206.
11. Haynes, W. M., *CRC handbook of chemistry and physics*. CRC press: 2014.
12. Kilpatrick, M.; Eanes, R. D., The dissociation constants of acids in salt solutions. II. Acetic acid. *J. Am. Chem. Soc.* **1953**, *75* (3), 586-587.
13. Eigen, M.; Schoen, J., Stoßspannungsverfahren zur Untersuchung sehr schnell verlaufender Ionenreaktionen in wässriger Lösung. *Ber. Bunsen. Phys. Chem.* **1955**, *59* (6), 483-494.
14. Eigen, M.; Eyring, E. M., Fast protolytic reactions in aqueous solutions of aminobenzoic acids. *J. Am. Chem. Soc.* **1962**, *84* (17), 3254-3256.
15. Staples†, B. R.; Turner‡, D. J.; Atkinson, G., An Apparatus for the Determination of Rates of Proton Transfer and Other Very Fast Reactions. *Instrum. Sci. Technol.* **1969**, *2* (2), 127-147.

16. Eyring, E. M.; Auburn, J. J.; Warrick Jr, P., Spectrophotometric dissociation field effect kinetics of aqueous acetic acid and bromocresol green. *J. Phys. Chem.* **1971**, *75* (16), 2488-2492.
17. Levich, V. G., Physicochemical hydrodynamics. **1962**.
18. Albery, W. J.; Bell, R. P., The Kinetics of the Dissociation of Weak Acids measured by a Rotating Platinum Disc Electrode. *Proc. Chem. Soc* **1963**, (June), 157-188.
19. Cohn, E. J.; Heyroth, F. F.; Menkin, M. F., THE DISSOCIATION CONSTANT OF ACETIC ACID AND THE ACTIVITY COEFFICIENTS OF THE IONS IN CERTAIN ACETATE SOLUTIONS. *J. Am. Chem. Soc.* **1928**, *50* (3), 696-714.
20. Ferra, M. I. A.; Graça, J. R.; Marques, A. M. M., Ionization of Acetic Acid in Aqueous Potassium Chloride Solutions. *J. Chem. Eng. Data* **2011**, *56* (9), 3673-3678.
21. Bruckenstein, S.; Nelson, D., Acid-Base Dissociation Constants in 1.0 M Sodium Chloride. *J. Chem. Eng. Data* **1961**, *6* (4), 605-606.
22. Vielstich, W.; Jahn, D., II7. Zur Messung schneller Reaktionen in Lösung mit Hilfe der rotierenden Scheibenelektrode. *Ber. Bunsen. Phys. Chem.* **1960**, *64* (1), 43-44.
23. Delahay, P.; Vielstich, W., Kinetics of the Dissociation of Weak Acids and Bases—Application of Polarography and Voltammetry at Constant Current. *J. Am. Chem. Soc.* **1955**, *77* (19), 4955-4958.
24. Barker, G.; Nürnberg, H. W., On the study of very rapid homogeneous chemical reactions by new electrochemical methods. *Naturwissenschaften* **1964**, *51* (8), 191-191.
25. Nürnberg, H.; Barker, G., The determination of the rate constants for the dissociation and recombination of weak acids by high level faradaic rectification. *Naturwissenschaften* **1964**, *51* (8), 191-192.
26. Zwaschka, G.; Tong, Y.; Wolf, M.; Kramer Campen, R., Probing the Hydrogen Evolution Reaction and Charge Transfer on Platinum Electrodes on Femtosecond Timescales. *ChemElectroChem* **2019**, *6* (10), 2675-2682.
27. Tavares, M. C.; Machado, S. A. S.; Mazo, L. H., Study of hydrogen evolution reaction in acid medium on Pt microelectrodes. *Electrochim. Acta* **2001**, *46* (28), 4359-4369.
28. Jiao, X.; Batchelor-McAuley, C.; Kätelhön, E.; Ellison, J.; Tschulik, K.; Compton, R. G., The subtleties of the reversible hydrogen evolution reaction arising from the nonunity stoichiometry. *J. Phys. Chem. C* **2015**, *119* (17), 9402-9410.
29. Gomez-Gil, J. M.; Laborda, E.; Molina, A., General Explicit Mathematical Solution for the Voltammetry of Nonunity Stoichiometry Electrode Reactions: Diagnosis Criteria in Cyclic Voltammetry. *Anal Chem* **2020**, *92* (5), 3728-3734.
30. Bard, A., *Standard potentials in aqueous solution*. Routledge: 2017.
31. Robinson, R. A.; Stokes, R. H., The Measurements and Interpretations of Conductance, Chemical Potential and Diffusion in Solutions of Simple Electrolytes. In *Electrolyte solutions*, Courier Corporation: 2002.
32. Wilhelm, E.; Battino, R.; Wilcock, R. J., Low-pressure solubility of gases in liquid water. *Chem. Rev.* **1977**, *77* (2), 219-262.
33. Long, F.; McDevit, W., Activity coefficients of nonelectrolyte solutes in aqueous salt solutions. *Chem. Rev.* **1952**, *51* (1), 119-169.
34. Li, X.; Batchelor-McAuley, C.; Novev, J. K.; Compton, R. G., A thermostated cell for electrochemistry: minimising natural convection and investigating the role of evaporation and radiation. *Phys. Chem. Chem. Phys.* **2018**, *20* (17), 11794-11804.
35. Wang, Y.; Limon-Petersen, J. G.; Compton, R. G., Measurement of the diffusion coefficients of $[\text{Ru}(\text{NH}_3)_6]^{3+}$ and $[\text{Ru}(\text{NH}_3)_6]^{2+}$ in aqueous solution using microelectrode double potential step chronoamperometry. *J. Electroanal. Chem.* **2011**, *652* (1), 13-17.
36. Compton, R. G.; Laborda, E.; Kaetelhoe, E.; Ward, K. R., *Understanding voltammetry: simulation of electrode processes*. 2nd ed.; World Scientific London, 2020.
37. Kätelhön, E.; Compton, R. G., Testing and validating electroanalytical simulations. *Analyst* **2015**, *140* (8), 2592-2598.
38. Kätelhön, E.; Compton, R. G., Correction: Testing and validating electroanalytical simulations. *Analyst* **2015**, *140* (9), 3290-3290.
39. Kätelhön, E.; Compton, R. G., Correction: Testing and validating electroanalytical simulations. *Analyst* **2016**, *141* (3), 1154-1154.
40. Abadi, M.; Barham, P.; Chen, J.; Chen, Z.; Davis, A.; Dean, J.; Devin, M.; Ghemawat, S.; Irving, G.; Isard, M. In *Tensorflow: A system for large-scale machine learning*, 12th {USENIX} symposium on operating systems design and implementation ({OSDI} 16), 2016; pp 265-283.
41. Philipp, G.; Song, D.; Carbonell, J. G., The exploding gradient problem demystified-definition, prevalence, impact, origin, tradeoffs, and solutions. *arXiv preprint arXiv:1712.05577* **2017**.
42. Daniele, S.; Lavagnini, I.; Baldo, M. A.; Magno, F., Steady state voltammetry at microelectrodes for the hydrogen evolution from strong and weak acids under pseudo-first and second order kinetic conditions. *J. Electroanal. Chem.* **1996**, *404* (1), 105-111.
43. Bockris, J. O. M.; Potter, E. C., The Mechanism of the Cathodic Hydrogen Evolution Reaction. *J. Electrochem. Soc.* **1952**, *99* (4), 169.
44. Juodkazytė, J.; Juodkasis, K.; Juodkasis, S., Atoms vs. Ions: Intermediates in Reversible Electrochemical Hydrogen Evolution Reaction. *Catalysts* **2021**, *11* (9), 1135.
45. Ma, R.; Wang, Y.; Li, G.; Yang, L.; Liu, S.; Jin, Z.; Zhao, X.; Ge, J.; Xing, W., Tuning the oxidation state of Ru to surpass Pt in hydrogen evolution reaction. *Nano Res.* **2021**.
46. Niu, S.; Yang, J.; Qi, H.; Su, Y.; Wang, Z.; Qiu, J.; Wang, A.; Zhang, T., Single-atom Pt promoted Mo2C for electrochemical hydrogen evolution reaction. *J. Energy Chem.* **2021**, *57*, 371-377.
47. Dubouis, N.; Grimaud, A., The hydrogen evolution reaction: from material to interfacial descriptors. *Chem. Sci.* **2019**, *10* (40), 9165-9181.
48. Pohl, M. D.; Watzele, S.; Calle-Vallejo, F.; Bandarenka, A. S., Nature of Highly Active Electrocatalytic Sites for the Hydrogen Evolution Reaction at Pt Electrodes in Acidic Media. *ACS Omega* **2017**, *2* (11), 8141-8147.
49. Koster, D.; Zeradjanin, A. R.; Battistel, A.; La Mantia, F., Extracting the kinetic parameters of the hydrogen evolution reaction at Pt in acidic media by means of dynamic multi-frequency analysis. *Electrochim. Acta* **2019**, *308*, 328-336.
50. Watzele, S.; Fichtner, J.; Garlyyev, B.; Schwämmlein, J. N.; Bandarenka, A. S., On the Dominating Mechanism of the Hydrogen Evolution Reaction at Polycrystalline Pt Electrodes in Acidic Media. *ACS Catalysis* **2018**, *8* (10), 9456-9462.
51. Kingma, D. P.; Ba, J., Adam: A method for stochastic optimization. *arXiv preprint arXiv:1412.6980* **2014**.
52. Efron, B., Bootstrap methods: another look at the jackknife. In *Breakthroughs in statistics*, Springer: 1992; pp 569-593.
53. Dunn, L.; Stokes, R., The diffusion of monocarboxylic acids in aqueous solution at 25°. *Aust. J. Chem.* **1965**, *18* (3), 285-296.
54. Miao, R.; Compton, R. G., The Electro-Oxidation of Hydrazine: A Self-Inhibiting Reaction. *The Journal of Physical Chemistry Letters* **2021**, *12* (6), 1601-1605.
55. Miao, R.; Shao, L.; Compton, R. G., Single entity electrochemistry and the electron transfer kinetics of hydrazine oxidation. *Nano Research* **2021**.
56. Li, D.; Batchelor-McAuley, C.; Compton, R. G., Voltammetry in sheep's blood: amperometric measurement of oxygen concentration. *Unpublished work* **2021**.
57. Gibson, Q. H.; Roughton, F. J. W., The kinetics of dissociation of the first oxygen molecule from fully saturated oxyhaemoglobin in sheep blood solutions. *Proc. R. Soc. London* **1955**, *143* (912), 310-334.
58. Roughton, F. J. W.; Otis, A.; Lyster, R., The determination of the individual equilibrium constants of the four intermediate reactions between oxygen and sheep haemoglobin. *Proc. R. Soc. London* **1955**, *144* (914), 29-54.

